

Discovery of the First Five Carbon-Enhanced Metal-Poor Stars in the LMC

MADELINE LUCEY ,¹ VEDANT CHANDRA ,² ALEXANDER P. JI ,^{3, 4, 5} ANDREW R. CASEY ,^{6, 7} DAVID NIDEVER ,⁸ SEAN MORRISON ,⁹ ROBYN E. SANDERSON ,¹⁰ SLATER ODEN ,⁸ JOSÉ G. FERNÁNDEZ-TRINCADO ,^{11, 12} AND GUILHERME LIMBERG ,^{3, 4}

¹ Department of Physics & Astronomy, University of Pennsylvania, 209 S 33rd St., Philadelphia, PA 19104, USA

² Center for Astrophysics | Harvard & Smithsonian, 60 Garden St, Cambridge, MA 02138, USA

³ Department of Astronomy & Astrophysics, University of Chicago, 5640 S Ellis Avenue, Chicago, IL 60637, USA

⁴ Kavli Institute for Cosmological Physics, University of Chicago, Chicago, IL 60637, USA

⁵ NSF-Simons AI Institute for the Sky (SkAI), 172 E. Chestnut St., Chicago, IL 60611, USA

⁶ School of Physics & Astronomy, Monash University, Wellington Road, Clayton, Victoria 3800, Australia

⁷ Center for Computational Astrophysics, Flatiron Institute, 162 Fifth Avenue, New York, NY 10010, USA

⁸ Department of Physics, Montana State University, P.O. Box 173840, Bozeman, MT 59717, USA

⁹ Department of Astronomy, University of Illinois at Urbana-Champaign, Urbana, IL 61801, USA

¹⁰ Department of Physics & Astronomy, University of Pennsylvania, 209 S 33rd St., Philadelphia, PA 19104, USA

¹¹ Universidad Católica del Norte, Núcleo UCN en Arqueología Galáctica - Inst. de Astronomía, Av. Angamos 0610, Antofagasta, Chile

¹² Universidad Católica del Norte, Departamento de Ingeniería de Sistemas y Computación, Av. Angamos 0610, Antofagasta, Chile

ABSTRACT

A substantial fraction of metal-poor stars in the local Milky Way halo exhibit large overabundances of carbon. These stars, dubbed Carbon-Enhanced Metal-Poor (CEMP) stars, provide crucial constraints on the nature of the early universe including the earliest nucleosynthetic events. Whether these stars exist at similar rates in nearby galaxies is a major open question with implications for the environmental dependence of early chemical evolution. Here, we present the discovery of the first five CEMP stars in the Milky Way's largest dwarf companion, the LMC, using SDSS-V spectra from the BOSS instrument. We measure metallicities ranging from $[\text{Fe}/\text{H}] = -2.1$ to -3.2 and evolutionary state corrected carbon enhancements of $[\text{C}/\text{Fe}] = +1.2$ to $+2.4$, placing these stars among the most metal-poor and carbon-rich ever identified in the LMC. This discovery demonstrates that CEMP stars do exist in the LMC despite previous null detections, and establishes the foundation for measuring the CEMP occurrence rate in this system. Such measurements will provide critical tests of whether environmental differences affect the formation channels and frequencies of these ancient, carbon-rich stars.

1. INTRODUCTION

The chemistry of stellar atmospheres acts as a fossil record, as it generally remains unchanged over a star's lifetime except in cases of binary mass transfer or certain late-stage evolutionary processes in giant stars. Metal-poor stars formed from gas with few metals, likely before the universe had undergone significant metal enrichment. Their compositions therefore provide direct constraints on the nucleosynthetic yields of the first stellar generations and the chemical evolution of the early universe (Beers & Christlieb 2005; Frebel & Norris 2015; Bonifacio et al. 2025).

Early studies of metal-poor stars discovered that a significant fraction exhibit a large overabundance of carbon ($[\text{C}/\text{Fe}] > 0.7$; Beers et al. 1992; Rossi et al. 1999; Beers & Christlieb 2005; Lucatello et al. 2006; Christlieb et al. 2008). The occurrence rate of these stars, referred to

as carbon-enhanced metal-poor (CEMP) stars, increases at lower metallicities, making up 10-30% of stars with $[\text{Fe}/\text{H}] < -2$ and $\approx 80\%$ with $[\text{Fe}/\text{H}] < -4$ in the local Galactic halo (Lucatello et al. 2006; Lee et al. 2013; Placco et al. 2014; Yoon et al. 2018; Placco et al. 2018; Limberg et al. 2021).

CEMP stars are further divided into a number of subclasses based on their neutron-capture element abundances (Beers & Christlieb 2005; Frebel 2018). Stars that exhibit enhancements in slow neutron-capture (*s*-process) elements (e.g., Ba) are dubbed CEMP-*s* stars. A small number of CEMP stars show enhancements in rapid neutron-capture (*r*-process) elements (e.g., Eu) which are called CEMP-*r* stars. CEMP-*r/s* stars exhibit enhancements in both *r*- and *s*-process elements (Gull et al. 2018), while CEMP-*i* stars exhibit enhancements of intermediate neutron-capture (*i*-process) ele-

ments (Frebel 2018). Lastly, CEMP-no stars do not exhibit any enhancements in neutron-capture elements. CEMP-no and CEMP-*s* are the most common sub-classes while CEMP-*r*, CEMP-*r/s* and CEMP-*i* are more rare (e.g., Zepeda et al. 2023).

The different sub-classes of CEMP stars are thought to be tied to different origin scenarios. CEMP-*s* stars, which are more common at $[\text{Fe}/\text{H}] > -2.5$, are thought to be related to mass-transfer events from (post-)asymptotic giant branch (AGB) stars (Lugardo et al. 2012; Placco et al. 2013). Some of the strongest evidence for this hypothesis lies in the high binarity rate of CEMP-*s* stars (McClure & Woodsworth 1990; Preston & Sneden 2001; Lucatello et al. 2005; Bisterzo et al. 2010; Abate et al. 2015; Hansen et al. 2016a; Jorissen et al. 2016). Hansen et al. (2016a) find that CEMP-*s* stars have a binarity rate as high as 82%.

CEMP-no stars, on the other hand, have a lower binary fraction and are therefore thought to be unrelated to binary evolution (Starkenburg et al. 2014; Hansen et al. 2016b; Arentsen et al. 2019). Their excess carbon is thus likely a natal property of CEMP-no stars, indicating they formed from carbon-rich gas. Furthermore, given their high occurrence rate at the lowest metallicities, enhanced carbon yields may be characteristic of the first supernovae. Recent observations of carbon enrichment in early galaxies with *JWST* provide further support for this scenario (D'Eugenio et al. 2024). Two theoretical explanations have been proposed for carbon over-production in the first supernovae: rapid rotation in the first stars (Chiappini et al. 2006; Meynet et al. 2006), or explosion as faint supernovae (Umeda & Nomoto 2003; Nomoto et al. 2013; Tominaga et al. 2014). Further studies of CEMP-no stars will help distinguish between these scenarios.

One major clue may lie in the environmental dependence of CEMP stars. Contrary to naive expectations based on where the oldest stars are thought to concentrate (El-Badry et al. 2018), CEMP stars are observed at lower rates in the inner Galaxy compared to the local halo (Howes et al. 2014, 2015, 2016; Arentsen et al. 2021; Lucey et al. 2022). Furthermore, while CEMP-no stars are found in ultra-faint dwarf galaxies at similar or higher rates to the Milky Way's halo, dwarf spheroidal galaxies exhibit a clear deficit (Norris et al. 2010; Lai et al. 2011; Frebel et al. 2014; Skúladóttir et al. 2015; Salvadori et al. 2015; Ji et al. 2020; Lucchesi et al. 2024; Sestito et al. 2024; Chiti et al. 2025). However, selection biases may drive these discrepant occurrence rates. Claimed deficits occur in more metal-rich environments where metallicity-sensitive photometric targeting methods are used to study the metal-poor stars, which are

biased against selecting CEMP stars (Da Costa et al. 2019; Chiti et al. 2020; Placco et al. 2025). Lucey et al. (2023) employed *Gaia* low-resolution XP spectra to detect an unbiased, full-sky sample of candidate CEMP stars and found their density peaks towards the Galactic center. Furthermore, Lucey et al. (2023) found a high density of candidate CEMP stars in the LMC and SMC, the Milky Way's largest dwarf galaxy companions. However, higher-resolution ($R \gtrsim 2,000$) spectroscopic follow-up is required to confirm these findings.

The LMC represents a unique opportunity to test the environmental dependence of CEMP. With a virial mass of $1 - 2 \times 10^{11} M_{\odot}$ and stellar mass of $3 \times 10^9 M_{\odot}$ (Kim et al. 1998; van der Marel et al. 2002; Erkal et al. 2019; Shipp et al. 2021; Watkins et al. 2024), the LMC is only one order of magnitude less massive than the Milky Way. The metallicity distribution of the LMC peaks at $[\text{Fe}/\text{H}] = -0.4$ to -0.65 , with only 10% of stars having $[\text{Fe}/\text{H}] < -1.0$ (Cole et al. 2005; Nidever et al. 2020). Detailed abundances for very metal-poor ($[\text{Fe}/\text{H}] < -2$) LMC stars have only recently been measured (Nidever et al. 2020; Reggiani et al. 2021; Chiti et al. 2024; Ji et al. 2025; Limberg et al. 2025), and no CEMP stars have yet been detected. However, confirming whether the LMC truly exhibits a lower occurrence rate of CEMP requires larger, unbiased samples.

The fifth-generation Sloan Digital Sky Survey (SDSS-V; Kollmeier et al. 2026) provides such a sample through its Magellanic Genesis program offering uniformly analyzed spectra for a large number of LMC stars, with limited targeting bias (Nidever et al. in prep). Here, we present the discovery of five CEMP stars in the LMC from this survey. In Section 2, we introduce the data including a short description of the target selection. Section 3 presents the spectroscopic analysis and in Section 4, we contextualize this discovery relative to LMC and Milky Way literature. Finally, Section 5 summarizes this work and the conclusions.

2. SDSS-V BOSS SPECTRA

SDSS-V includes observations with the Baryons Oscillation Spectroscopic Survey (BOSS) spectrograph (Smee et al. 2013). These spectra have $R \approx 1800$ and wavelength coverage from 3650–9000 Å. The spectra used in this work are from the 2.5m duPont telescope at Las Campanas Observatory (LCO) (Bowen & Vaughan 1973). The spectra were reduced using `IDLspec2D v6_2_1` (Bolton et al. 2012; Dawson et al. 2013, Morrison et al. in prep) with coadds and continuum normalization performed by the `astra` pipeline (Casey et al. in prep).

2.1. Magellanic Genesis Program

For a full description of the Magellanic Genesis program in SDSS-V, we refer the reader to Nidever et al. (in prep). Here, we briefly describe the targeting selection for the survey. The data used in this work specifically come from the red giant branch (RGB) selection which are selected using a 10-sided polygon in *Gaia* G and BP–RP with a bright limit of G=17.5 mag (see Figure 7 in Nidever et al. in prep). The Magellanic Genesis program also applies a spatial selection, including only stars within 30° of (RA, DEC)=(80.8925° , -72.1849°). In addition, the program utilizes the following proper motion cut to remove contamination from Milky Way stars:

$$(\mu_{LMS} - 1.8)^2 + (\mu_{BMS} - 0.4)^2 < 1.22 \quad (1)$$

where μ_{LMS} and μ_{BMS} are the proper motions in Magellanic Stream coordinates (Nidever et al. 2008).

Figure 1 shows the sky positions and proper motions in Magellanic Stream coordinates (Nidever et al. 2008) of our five CEMP stars (red stars) relative to the rest of the SDSS-V DR20 BOSS data. Four of our stars are located near the edges of the LMC disk, while the fifth star is more in the halo of the LMC. The proper motions are all consistent with being part of the Magellanic system. Radial velocities (RVs; see Table 1) as measured by the BOSS-MINESweeper pipeline (see Section 3.1; Chandra et al. 2025) are also consistent with the LMC system. BOSS-MINESweeper RVs from LCO spectra are offset from those derived by the higher-resolution APOGEE spectra by an average of 9 km/s. This is due to a known wavelength calibration issue, for further discussion we refer the reader to Section 3.2 of Chandra et al. (2025).

3. SPECTRAL ANALYSIS

In this work, we analyze five mid-resolution optical spectra from the SDSS-V BOSS instrument. First, we obtain estimates for the effective temperature (T_{eff}), surface gravity ($\log g$), and metallicity ([Fe/H]) using the MINEsweeper pipeline, which produces stellar parameters for all stars in the SDSS-V halo survey (Cargile et al. 2020; Chandra et al. 2025). We then provide a secondary constraint on the metallicity by fitting the Ca II infrared triplet. Last, we estimate the carbon abundances using spectral fitting to carbon molecular features.

3.1. MINEsweeper Parameters

Stellar parameters for the SDSS-V halo survey are derived using the MINEsweeper pipeline, producing the

BOSS-MINEsweeper value-added catalog¹ (Cargile et al. 2020; Chandra et al. 2025). For a full description of the BOSS-MINEsweeper catalog, we refer the reader to Chandra et al. (2025). As a short overview, the MINEsweeper pipeline performs Bayesian inference to estimate the effective temperature (T_{eff}), surface gravity ($\log g$), [Fe/H], [α/Fe], projected rotation velocity ($V_* \sin i$), initial mass ($M_{*,\text{initial}}$), age, distance and extinction (A_V). In addition to the BOSS spectra, the pipeline fits 2MASS, SDSS, Pan-STARRS, WISE, and *Gaia* photometry, along with *Gaia* parallaxes, where available (Fukugita et al. 1996; Gunn et al. 1998; Skrutskie et al. 2006; Mainzer et al. 2014; Chambers et al. 2016; Gaia Collaboration et al. 2021, 2023). The parameters are constrained to follow MIST isochrones, restricting solutions to physically-plausible regions of the parameter space (Dotter 2016; Choi et al. 2016). The model spectra are synthesized in 1D LTE using the radiative transfer codes ATLAS12 and SYNTHE (Kurucz 1970; Kurucz & Avrett 1981; Kurucz 1993).

The nominal BOSS-MINEsweeper analysis fits the spectra in the wavelength range 4750–5550 Å. Although this is a fraction of the available BOSS wavelength range, the model spectra have been empirically calibrated in this region to deliver reliable parameters. For this work, we include a mask to remove the region between 5060–5180 Å where a C_2 Swan band dominates. The MINEsweeper pipeline does not vary carbon and therefore cannot accurately model this region for carbon-enhanced stars. In order to ensure that this doesn't bias the results, we remove this region from the fit.

There are approximately 21,500 stars with reliable MINEsweeper parameters in the SDSS-V DR20 Magellanic Genesis catalog. Of these, 381 are CEMP candidates based on their *Gaia* XP spectra (Lucey et al. 2023). We then narrow it down to 5 stars for detailed analysis using preliminary fits to the CH G band and MINEsweeper metallicities, picking the cleanest stars with the lowest metallicities and largest [C/Fe].

The MINEsweeper-derived T_{eff} and $\log g$ of our five CEMP stars (black stars) relative to the rest of the SDSS-V DR20 Magellanic Genesis sample (colored by [Fe/H]) is shown in Figure 2. The Magellanic Genesis sample is designed to target RGB stars and in order to achieve sufficient SNR, they tend to be luminous stars with low $\log g$. Our five CEMP stars lie on the hottest end of the RGB, consistent with being very metal-poor.

¹ Public catalogs are available with each SDSS data release here: https://www.sdss.org/dr19/data_access/value-added-catalogs/?vac_id=10007

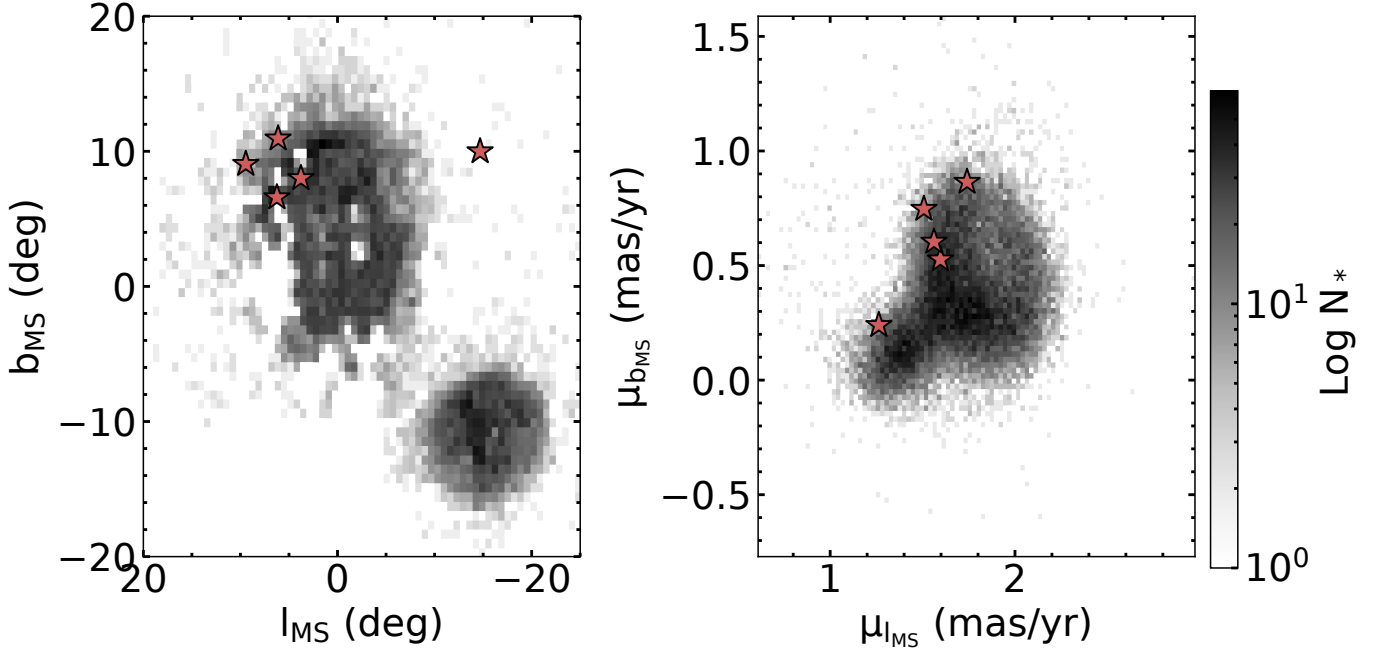


Figure 1. Distribution of sky positions (left panel), and proper motions (right panel) in Magellanic Stream coordinates (Nidever et al. 2008) of the five CEMP stars (red stars) relative to the rest of the Magellanic Clouds sample in SDSS-V DR20. All five stars have sky coordinates and proper motions consistent with LMC membership.

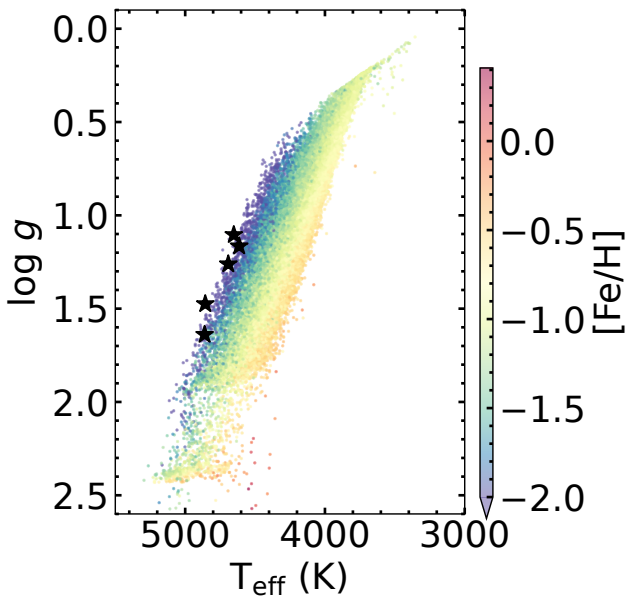


Figure 2. The **MINESweeper** stellar parameters for our five CEMP stars (black stars) relative to the rest of the SDSS-V DR20 Magellanic Genesis sample which is colored by metallicity. The five stars lay on the hotter edge of the red giant branch (RGB), consistent with having some of the lowest metallicities in the sample.

3.2. *Ca II Triplet Metallicity Estimates*

To validate and further constrain the metallicity estimates for these stars we fit the two strongest Ca II infrared triplet lines at 8542 Å and 8662 Å. Throughout this work, we linearly interpolate synthetic spectra models. We used a synthetic spectrum grid of red giant stars computed in 1D LTE using Turbospectrum (Plez 2012), spherical MARCS model atmospheres (Gustafsson et al. 2008), and the VALD atomic data (Ryabchikova et al. 2015). The grid was synthesized using 32,678 randomly chosen red giant surface gravities from $0 < \log g < 3.5$ with a large range of effective temperatures corresponding to a metal-poor Dartmouth isochrone (Dotter et al. 2008).

We utilize these models to estimate the [Ca/H]. See Appendix A for more details on the spectral fitting. To convert this to [Fe/H], we assume a $[\alpha/\text{Fe}]$ value. We do not use the $[\alpha/\text{Fe}]$ from **MINESweeper** in order to achieve an independent estimate of the [Fe/H]. Instead, we use the median [Ca/Fe] value from Chiti et al. (2024) which measures abundances for stars in a similar metallicity range as this work (see Section 4) using high-resolution optical spectra from Magellan/MIKE. The median [Ca/Fe] abundance from that work is 0.24 dex with a standard deviation of 0.14 dex. The full range of [Ca/Fe] abundances is 0.02-0.48 dex. Therefore, we adopt [Ca/Fe] of 0.24 dex and estimate the [Fe/H] as [Ca/H]-0.24.

The primary source of uncertainty for this [Fe/H] estimates comes from the [Ca/Fe] assumption. To be conservative we estimate the uncertainty on the [Ca/Fe] as 2 times the standard deviation of the [Ca/Fe] abundances from Chiti et al. (2024) which is 0.28 dex. We add this in quadrature with the variance from the spectral fitting.

The [Fe/H] estimates from the Ca II triplet generally agree with the [Fe/H] from **MINESweeper** with all of the differences being within 0.51 dex (see Appendix A). For the final [Fe/H] estimates, we take the average of the two measurements. The uncertainty is then calculated using standard error propagation given two independent measurements.

3.3. Carbon Abundance Estimates

Using the same synthetic spectra fitting procedure as above, we derive the carbon abundance in two regions, the CH G band between 4280-4350 Å and a C₂ Swan band between 5050-5200 Å. We perform the fit to the regions simultaneously to achieve consistent estimates. Figures of the fits to each feature are included in Appendix B.

In Figure 3, we show the synthetic spectral fit (blue) overlaid on the observed spectra (grey) for each of the five CEMP stars. We label the CH G-band at 4505 Å and the C₂ Swan band at 5165Å that we fit to derive the carbon abundance. The T_{eff} and $\log g$ are fixed to values from the **MINESweeper** pipeline. The [Fe/H] is the average between the **MINESweeper** value and the value estimated from the Ca II infrared Triplet (see Section 3.2). In general, the model spectra fit the observed spectra well.

The largest source of uncertainty comes from uncertainty on the stellar parameters, T_{eff} , $\log g$ and [Fe/H]. To account for this, we recalculate the carbon abundance for each star given the stellar parameter uncertainties. We do this twice for each star, in the cooler star ($T_{\text{eff,cool}} = T_{\text{eff}} - \sigma_{T_{\text{eff}},l}$, $\log g_{\text{cool}} = \log g - \sigma_{\log g,l}$, $[\text{Fe}/\text{H}]_{\text{cool}} = [\text{Fe}/\text{H}] - \sigma_{[\text{Fe}/\text{H}]}$) and warmer star ($T_{\text{eff,hot}} = T_{\text{eff}} + \sigma_{T_{\text{eff}},h}$, $\log g_{\text{hot}} = \log g + \sigma_{\log g,h}$, $[\text{Fe}/\text{H}]_{\text{hot}} = [\text{Fe}/\text{H}] + \sigma_{[\text{Fe}/\text{H}]}$) scenario. We take the largest difference between the re-derived and fiducial values for each star as the respective stellar parameter propagated uncertainty. This is then combined in quadrature with the variance from the fits to the carbon molecular features to calculate the total uncertainty.

As stars evolve up the RGB, the convective mixing leads to a depletion of carbon in the atmosphere. Therefore, we apply evolutionary state corrections to account for this effect on the derived abundances following (Placco et al. 2014). The correction is a function of $\log g$, [Fe/H] and [C/Fe], with the correction being largest

for stars with low $\log g$, low [Fe/H] and low [C/Fe]. In general for our stars the corrections are on the order of 0.1-0.3 dex. Both the fit and corrected values are given in Table 1.

4. COMPARISON TO LITERATURE

To place our five CEMP LMC stars in context, we compare the measured abundances to literature samples from the LMC and the Milky Way. In Figure 4, we show the [C/Fe] as a function of metallicity for our five stars (black circles) relative to previous works in the LMC. In addition, the [C/Fe] abundances that include the correction for evolutionary state are shown in grey triangles. The dark blue points are abundances from Chiti et al. (2024), which targeted some of the most metal-poor stars in the LMC and also include the evolutionary state correction. In red, we show results from the SDSS-IV DR17 APOGEE catalog for the LMC (Nidever et al. 2020; Abdurro'uf et al. 2022). The APOGEE abundances do not include an evolutionary state correction. It is possible that some of the APOGEE DR17 stars would be considered CEMP if the evolutionary state corrections were calculated and applied. However, the spectra would need to be visibly inspected to confirm the results as the APOGEE abundance pipeline is not designed to handle CEMP stars. The five CEMP stars we report have substantially higher carbon abundances than ever previously measured in the LMC.

Without neutron-capture abundance estimates, we cannot assign these stars to specific CEMP subclasses. However, the absolute carbon abundance can be informative for classification (Yoon et al. 2016). In Figure 5, we show the absolute carbon abundance (A(C)), which includes the evolutionary state correction, as a function of metallicity for our five stars compared to Milky Way CEMP stars with known neutron-capture abundances compiled in Yoon et al. (2016). The literature CEMP stars with enhanced *s*-process ($[\text{Ba}/\text{Fe}] > 1$; CEMP-*s* stars) are shown as light blue circles, while the CEMP-no stars with $[\text{Ba}/\text{Fe}] < 0$ are shown in red circles. The black dashed line indicates [C/Fe]=0.7 dex. The grey dashed lines indicate the different classes defined by Yoon et al. (2016), with Group I in the top right, Group II in the bottom left and Group III in the top left. These groups are defined to capture the different structures in Figure 5. Group I encapsulates the blob of CEMP-*s* stars at higher metallicities and A(C). Group II represents the CEMP-no stars that have a roughly linear relationship between [Fe/H] and A(C), while Group III captures the CEMP-no stars with A(C)~7 at the lowest metallicities.

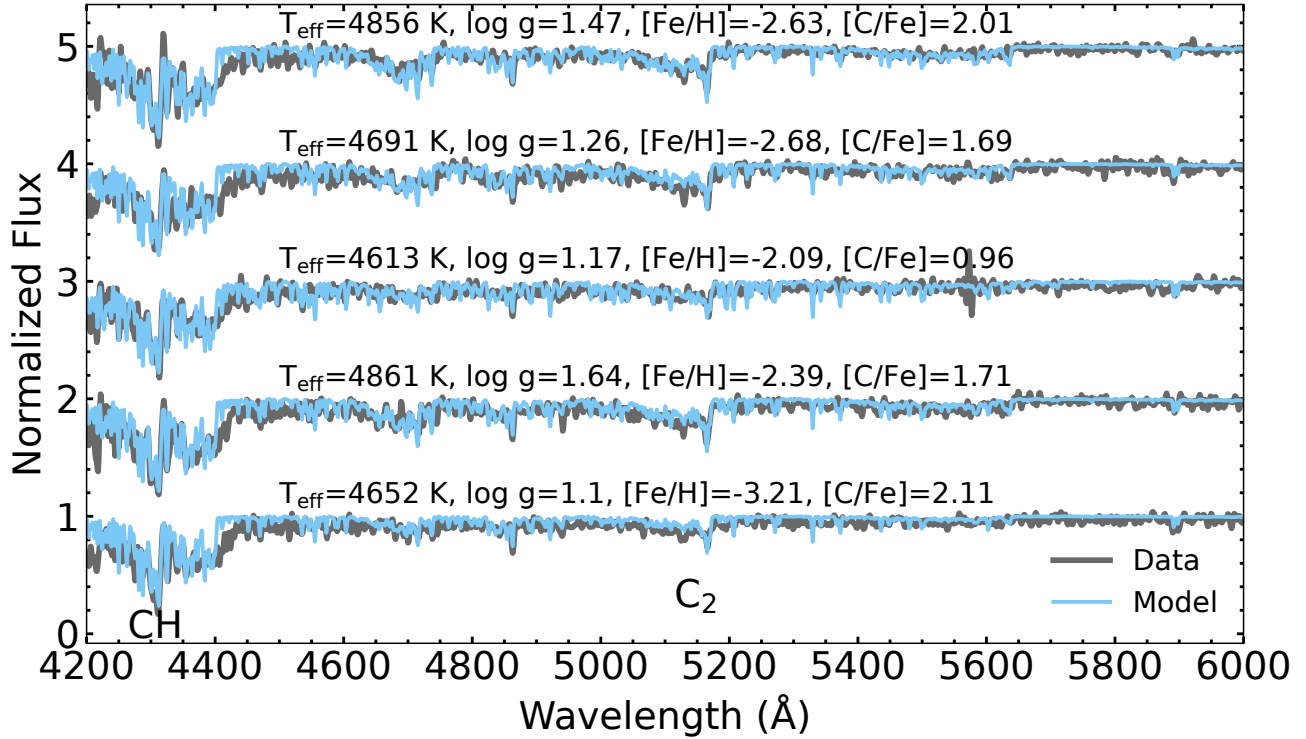


Figure 3. A region of the BOSS spectra (grey) for the five CEMP stars with the best-fit synthetic spectral model (blue) overlaid. The spectral models shown are used for fitting the carbon abundance while the T_{eff} and $\log g$ are fixed to the **MINESweeper** parameters. This region contains the CH G-band at 4305 Å and the C₂ Swan bands, with the strongest feature at 5165 Å. The **MINESweeper** analysis also uses a subset of this region (4750–5550 Å) for the stellar parameter analysis with a mask for the C₂ band at 5060–5180 Å.

Table 1. Sky Coordinates, and Stellar Parameters of the Five CEMP Stars

SDSS ID	RA (deg)	DEC (deg)	SNR (pixel ⁻¹)	RV (km/s)	T_{eff} (K)	$\log g$	[Fe/H]	[C/Fe]	[C/Fe] _{corr}
92278782	53.88	-58.18	28.12	175^{+12}_{-12}	4652^{+47}_{-42}	1.10^{+10}_{-09}	-3.21 ± 0.21	2.11 ± 0.30	2.41 ± 0.30
96041179	96.65	-65.10	20.93	244^{+17}_{-28}	4861^{+71}_{-65}	1.64^{+17}_{-15}	-2.39 ± 0.21	1.71 ± 0.14	1.85 ± 0.14
98320880	90.49	-64.07	25.01	291^{+11}_{-11}	4614^{+53}_{-52}	1.17^{+12}_{-12}	-2.09 ± 0.17	0.96 ± 0.39	1.23 ± 0.39
98332219	102.15	-61.90	20.46	317^{+10}_{-9}	4692^{+110}_{-61}	1.26^{+20}_{-13}	-2.68 ± 0.23	1.69 ± 0.11	2.05 ± 0.11
98357416	94.57	-60.84	31.74	295^{+8}_{-7}	4856^{+52}_{-53}	1.47^{+10}_{-11}	-2.63 ± 0.16	2.01 ± 0.20	2.17 ± 0.20

NOTE—The SDSS ID, right ascension (RA), declination (DEC), and Signal-to-Noise Ratio (SNR) of the BOSS spectra. The effective temperature (T_{eff}), and surface gravity ($\log g$) with associated uncertainties are from the **BOSS-MINESweeper** catalog. The derivations of the metallicity ([Fe/H], and carbon abundance ([C/Fe]) are described in Section 3.2 and 3.3, respectively.

All five of our LMC CEMP stars lie in the Group I region which indicates they may be CEMP-*s* stars. We likely only find Group I stars since we chose to focus our analysis on stars with the largest carbon abundances and therefore this result does not indicate anything about population rates in the LMC. Furthermore, higher-resolution spectra to confirm their neutron-capture element abundances are required. It is unclear whether this classification system would be appli-

cable beyond the Milky Way given the differences in chemical evolution between galaxies of various masses. There is already discussion on developing environment-dependent CEMP classification where the [C/Fe] cut-off scales with the average [C/Fe] of the system (e.g., [Sestito et al. 2024](#)).

5. SUMMARY AND CONCLUSIONS

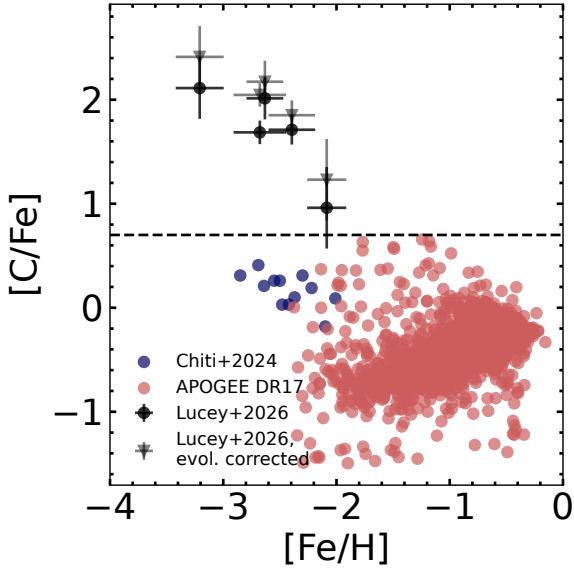


Figure 4. Carbon abundances ($[C/Fe]$) as a function of $[Fe/H]$ for the five CEMP stars compared to literature samples. Specifically, we compare to results from Chiti et al. (2024) which reports abundances for some of the most metal-poor stars known in the LMC, along with results from APOGEE spectra in SDSS-IV DR17. The commonly-used definition for CEMP ($[C/Fe] > 0.7$) is shown as a black dashed line, with the five stars from this work being the only stars above said line.

CEMP stars provide crucial constraints on early universe nucleosynthesis (Chiappini et al. 2006; Tominaga et al. 2014; D’Eugenio et al. 2024). Whether the occurrence rate of CEMP stars at low metallicities is dependent on the environment is an ongoing mystery that has interesting implications for the nature of the early universe and star formation. While CEMP stars are abundant at low-metallicities in the local Milky Way halo, and ultra-faint dwarf galaxies, there is an observational deficit in dwarf spheroidal galaxies, including no previous detections in the LMC (Lucchesi et al. 2024; Sestito et al. 2024; Chiti et al. 2024; Ji et al. 2025; Limberg et al. 2025). However, it is unclear whether this is a true discrepancy or whether photometric metallicity selection introduce biases (Da Costa et al. 2019; Chiti et al. 2020; Placco et al. 2025).

In this work, we use data from the SDSS-V Magellanic Genesis program to search for CEMP stars in the LMC. We identify CEMP candidates within the data using the catalog from Lucey et al. (2023). Of those for which reliable MINESweeper parameters were derived, we select five stars with the strongest carbon molecular features to derive abundances. Specifically, we measure carbon

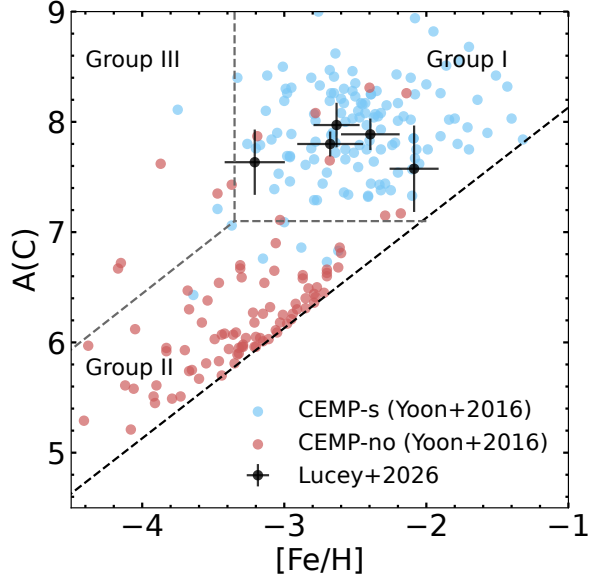


Figure 5. The absolute Carbon abundance ($A(C)$) as a function of $[Fe/H]$ for the five CEMP stars compared to a literature sample from the local Milky Way halo where the $[Ba/Fe]$ abundances are also measured. The literature sample is separated by $[Ba/Fe]$ where stars with $[Ba/Fe] > 1$ are labeled CEMP-s stars and are shown in blue while stars with $[Ba/Fe] \leq 0$ are labeled CEMP-no and are shown in red. The black dashed line indicates $[C/Fe] = 0.7$. The grey dashed lines indicate the classification system of CEMP introduced by Yoon et al. (2016), where Group I is the top right section and are mainly CEMP-s, Group II and III are the bottom and top left sections and are mainly CEMP-no stars.

using synthetic spectra fits to the CH G band and a C_2 Swan band.

With this method, we discover the first five CEMP stars in the LMC. Based on their absolute carbon abundances and metallicities, these stars are likely CEMP-s stars given the classification presented in Yoon et al. (2016). However, it is unclear whether this classification would apply beyond the Milky Way and therefore further observations to confirm the neutron-capture elements are required.

The discovery of these five stars represents a crucial step towards understanding the chemistry of the most metal-poor stars in the LMC. In future work, we plan to homogeneously analyze all of the BOSS spectra of the LMC and SMC from SDSS-V to robustly measure the occurrence rate of CEMP in these galaxies. In total, this, along with other upcoming LMC surveys (e.g., 4MOST 1001MC; Cioni et al. 2019), will bring new understanding to nucleosynthesis in the early universe, especially with respect to environmental effects.

APPENDIX

A. CA II INFRARED TRIPLET METALLICITIES

In addition to the `MINESweeper` analysis, we further constrain the metallicities of these stars by modeling the Ca II infrared triplet. This analysis provides an estimate of the [Ca/H] abundance which we then convert to [Fe/H], assuming a [Ca/Fe] abundance based on literature LMC abundances of similar metallicity stars (Chiti et al. 2024).

In Figure 6, we show the best-fit synthetic spectra model (blue dashed line) compared to the data (black line). The linearly interpolated synthetic spectra are described in Section 3. We fit a continuum normalization for the model spectra to best match the observed spectra which is shown as a red dashed line. Although the entire region shown is used for fitting the continuum, we use only the two strongest Ca lines (8542 Å and 8662 Å) to fit the abundance.

The comparison between the derived Ca triplet and `MINESweeper` metallicities are shown in Figure 7. They show good agreement with all differences within $\approx 2\sigma$. The star which shows the largest discrepancy (0.51 dex) is also the most metal-poor, and has a low SNR spectrum with few discernible absorption lines in the wavelength range fit by `MINESweeper`. For the final reported metallicity estimates we take the average of these two independent measurements and propagate the uncertainty accordingly.

B. FITS TO CARBON MOLECULAR FEATURES

To estimate the carbon abundance, we fit two molecular features, the CH G band at 4306 Å and a C₂ Swan band at 5165 Å. In Figure 8, we show the fits to the CH G band while in Figure 9 we show the C₂ Swan band fits. In both figures, the observed spectra are shown as black lines and the best fit model spectra are shown as blue dashed lines. The fits are very sensitive to the continuum normalization. To account for this, we refit the continuum normalization for the model spectra (red dashed line) to best match the observed.

Software: Astropy (Astropy Collaboration et al. 2013, 2018), Matplotlib (Hunter 2007), IPython (Pérez & Granger 2007), Numpy (Harris et al. 2020), Scipy (Virtanen et al. 2020), Gala (Price-Whelan 2017; Price-Whelan et al. 2025)

ACKNOWLEDGEMENTS

1 This material is based upon work supported by the National
 2 Science Foundation under Award No. 2303831.
 3 Funding for the Sloan Digital Sky Survey V has
 4 been provided by the Alfred P. Sloan Foundation, the
 5 Heising-Simons Foundation, the National Science Foundation, and the Participating Institutions. SDSS ac-
 6 knowledges support and resources from the Center for
 7 High-Performance Computing at the University of Utah.
 8 SDSS telescopes are located at Apache Point Observatory, funded by the Astrophysical Research Con-
 9 sortium and operated by New Mexico State University,
 10 and at Las Campanas Observatory, operated by the
 11 Carnegie Institution for Science. The SDSS web site
 12 is www.sdss.org.

13 SDSS is managed by the Astrophysical Research Con-
 14 sortium for the Participating Institutions of the SDSS
 15 Collaboration, including the Carnegie Institution for
 16 Science, Chilean National Time Allocation Commit-
 17 tee (CNTAC) ratified researchers, Caltech, the Gotham
 18 Participation Group, Harvard University, Heidelberg
 19 University, The Flatiron Institute, The Johns Hop-
 20 kins University, L'Ecole polytechnique fédérale de Lau-
 21 sanne (EPFL), Leibniz-Institut für Astrophysik Pots-
 22 dam (AIP), Max-Planck-Institut für Astronomie (MPIA
 23 Heidelberg), Max-Planck-Institut für Extraterrestrische
 24 Physik (MPE), Nanjing University, National Astronom-
 25 ical Observatories of China (NAOC), New Mexico State
 26 University, The Ohio State University, Pennsylvania
 27 State University, Smithsonian Astrophysical Observa-
 28 tory, Space Telescope Science Institute (STScI), the
 29 Stellar Astrophysics Participation Group, Universidad
 30 Nacional Autónoma de México, University of Arizona,
 31 University of Colorado Boulder, University of Illinois at
 32 Urbana-Champaign, University of Toronto, University
 33 of Utah, University of Virginia, Yale University, and
 34 Yunnan University.

35 This work has made use of data from the Euro-
 36 pean Space Agency (ESA) mission *Gaia* (<https://www.cosmos.esa.int/gaia>), processed by the *Gaia* Data Pro-
 37 cessing and Analysis Consortium (DPAC, <https://www.cosmos.esa.int/web/gaia/dpac/consortium>). Funding
 38 for the DPAC has been provided by national institu-
 39 tions, in particular the institutions participating in the
 40 *Gaia* Multilateral Agreement.

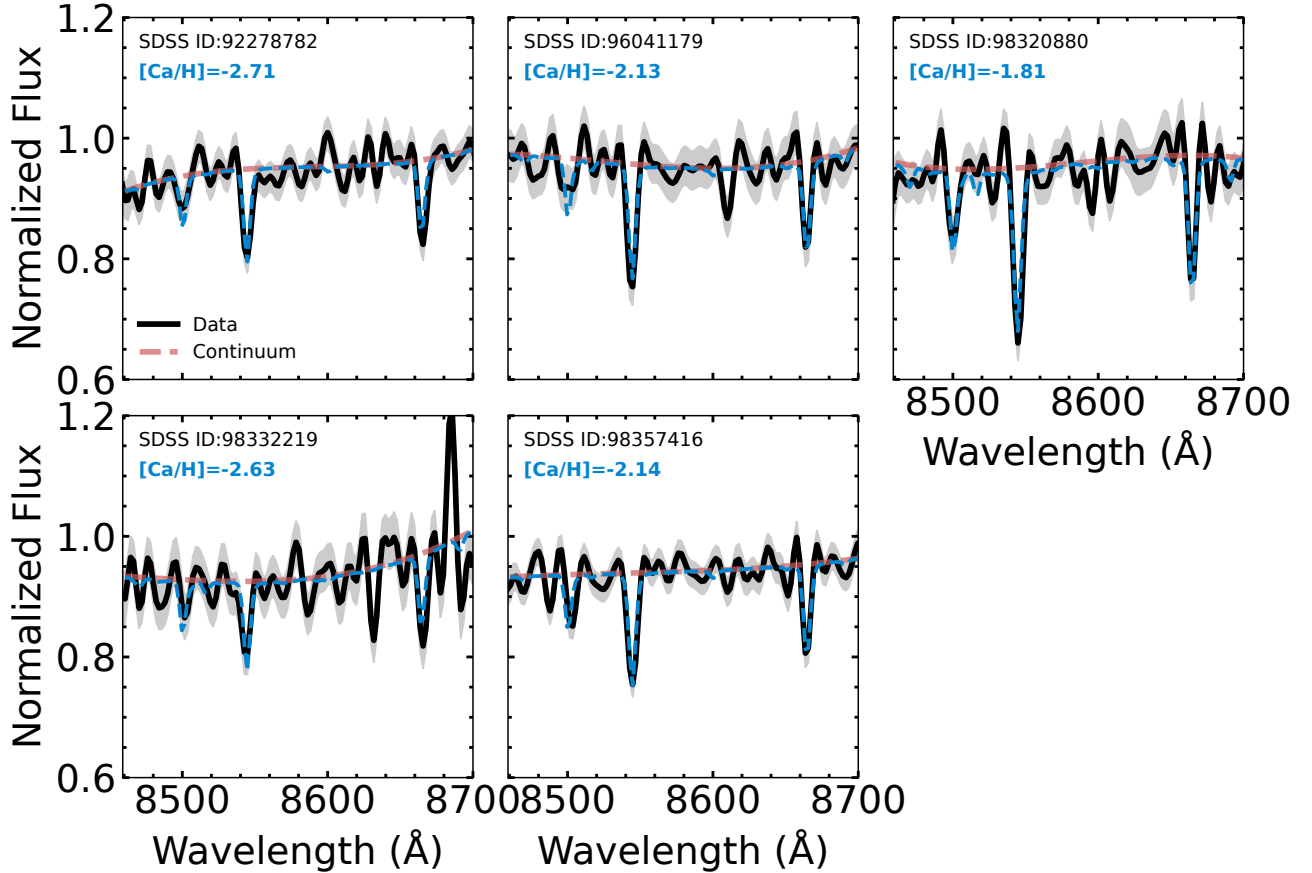


Figure 6. The fits to the Ca II infrared triplet for the five CEMP stars. The black line with the grey shaded region give the observed normalized flux and the corresponding uncertainty. The blue dashed lines is the best-fit synthetic spectra. As the fit is highly sensitive to the continuum normalization, we fit the model continuum to best match the observed spectra. The red dashed line gives the continuum normalization for the best-fit model.

REFERENCES

- Abate, C., Pols, O. R., Karakas, A. I., & Izzard, R. G. 2015, *A&A*, 576, A118, doi: [10.1051/0004-6361/201424739](https://doi.org/10.1051/0004-6361/201424739)
- Abdurro'uf, Accetta, K., Aerts, C., et al. 2022, *ApJS*, 259, 35, doi: [10.3847/1538-4365/ac4414](https://doi.org/10.3847/1538-4365/ac4414)
- Arentsen, A., Starkenburg, E., Shetrone, M. D., et al. 2019, *A&A*, 621, A108, doi: [10.1051/0004-6361/201834146](https://doi.org/10.1051/0004-6361/201834146)
- Arentsen, A., Starkenburg, E., Aguado, D. S., et al. 2021, *MNRAS*, 505, 1239, doi: [10.1093/mnras/stab1343](https://doi.org/10.1093/mnras/stab1343)
- Astropy Collaboration, Robitaille, T. P., Tollerud, E. J., et al. 2013, *A&A*, 558, A33, doi: [10.1051/0004-6361/201322068](https://doi.org/10.1051/0004-6361/201322068)
- Astropy Collaboration, Price-Whelan, A. M., Sipőcz, B. M., et al. 2018, *AJ*, 156, 123, doi: [10.3847/1538-3881/aabc4f](https://doi.org/10.3847/1538-3881/aabc4f)
- Beers, T. C., & Christlieb, N. 2005, *ARA&A*, 43, 531, doi: [10.1146/annurev.astro.42.053102.134057](https://doi.org/10.1146/annurev.astro.42.053102.134057)
- Beers, T. C., Preston, G. W., & Shectman, S. A. 1992, *AJ*, 103, 1987, doi: [10.1086/116207](https://doi.org/10.1086/116207)
- Bisterzo, S., Gallino, R., Straniero, O., Cristallo, S., & Käppeler, F. 2010, *MNRAS*, 404, 1529, doi: [10.1111/j.1365-2966.2010.16369.x](https://doi.org/10.1111/j.1365-2966.2010.16369.x)
- Bolton, A. S., Schlegel, D. J., Aubourg, É., et al. 2012, *AJ*, 144, 144, doi: [10.1088/0004-6256/144/5/144](https://doi.org/10.1088/0004-6256/144/5/144)
- Bonifacio, P., Caffau, E., François, P., & Spite, M. 2025, *A&A Rv*, 33, 2, doi: [10.1007/s00159-025-00159-2](https://doi.org/10.1007/s00159-025-00159-2)
- Bowen, I. S., & Vaughan, Jr., A. H. 1973, *ApOpt*, 12, 1430, doi: [10.1364/AO.12.001430](https://doi.org/10.1364/AO.12.001430)
- Cargile, P. A., Conroy, C., Johnson, B. D., et al. 2020, *ApJ*, 900, 28, doi: [10.3847/1538-4357/aba43b](https://doi.org/10.3847/1538-4357/aba43b)
- Chambers, K. C., Magnier, E. A., Metcalfe, N., et al. 2016, arXiv e-prints, arXiv:1612.05560, doi: [10.48550/arXiv.1612.05560](https://doi.org/10.48550/arXiv.1612.05560)

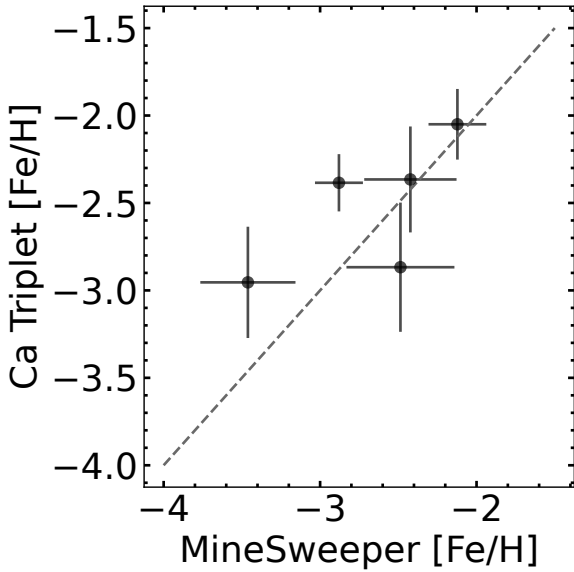


Figure 7. The metallicities derived from the Ca II triplet compared to the `MINEsweeper` metallicity. In general, the values show good agreement with the largest difference for the most metal-poor star being 0.51 dex. The final metallicities reported in this work is the average of these two values.

- Chandra, V., Cargile, P. A., Ji, A. P., et al. 2025, arXiv e-prints, arXiv:2508.00978, doi: [10.48550/arXiv.2508.00978](https://doi.org/10.48550/arXiv.2508.00978)
- Chiappini, C., Hirschi, R., Meynet, G., et al. 2006, A&A, 449, L27, doi: [10.1051/0004-6361:20064866](https://doi.org/10.1051/0004-6361:20064866)
- Chiti, A., Frebel, A., Jerjen, H., Kim, D., & Norris, J. E. 2020, ApJ, 891, 8, doi: [10.3847/1538-4357/ab6d72](https://doi.org/10.3847/1538-4357/ab6d72)
- Chiti, A., Mardini, M., Limberg, G., et al. 2024, Nature Astronomy, 8, 637, doi: [10.1038/s41550-024-02223-w](https://doi.org/10.1038/s41550-024-02223-w)
- Chiti, A., Placco, V. M., Pace, A. B., et al. 2025, arXiv e-prints, arXiv:2508.04053, doi: [10.48550/arXiv.2508.04053](https://doi.org/10.48550/arXiv.2508.04053)
- Choi, J., Dotter, A., Conroy, C., et al. 2016, ApJ, 823, 102, doi: [10.3847/0004-637X/823/2/102](https://doi.org/10.3847/0004-637X/823/2/102)
- Christlieb, N., Schörck, T., Frebel, A., et al. 2008, A&A, 484, 721, doi: [10.1051/0004-6361:20078748](https://doi.org/10.1051/0004-6361:20078748)
- Cioni, M. . R. L., Storm, J., Bell, C. P. M., et al. 2019, The Messenger, 175, 54, doi: [10.18727/0722-6691/5128](https://doi.org/10.18727/0722-6691/5128)
- Cole, A. A., Tolstoy, E., Gallagher, III, J. S., & Smecker-Hane, T. A. 2005, AJ, 129, 1465, doi: [10.1086/428007](https://doi.org/10.1086/428007)
- Da Costa, G. S., Bessell, M. S., Mackey, A. D., et al. 2019, MNRAS, 489, 5900, doi: [10.1093/mnras/stz2550](https://doi.org/10.1093/mnras/stz2550)
- Dawson, K. S., Schlegel, D. J., Ahn, C. P., et al. 2013, AJ, 145, 10, doi: [10.1088/0004-6256/145/1/10](https://doi.org/10.1088/0004-6256/145/1/10)

- D'Eugenio, F., Maiolino, R., Carniani, S., et al. 2024, A&A, 689, A152, doi: [10.1051/0004-6361/202348636](https://doi.org/10.1051/0004-6361/202348636)
- Dotter, A. 2016, ApJS, 222, 8, doi: [10.3847/0067-0049/222/1/8](https://doi.org/10.3847/0067-0049/222/1/8)
- Dotter, A., Chaboyer, B., Jevremović, D., et al. 2008, ApJS, 178, 89, doi: [10.1086/589654](https://doi.org/10.1086/589654)
- El-Badry, K., Bland-Hawthorn, J., Wetzel, A., et al. 2018, MNRAS, 480, 652, doi: [10.1093/mnras/sty1864](https://doi.org/10.1093/mnras/sty1864)
- Erkal, D., Belokurov, V., Laporte, C. F. P., et al. 2019, MNRAS, 487, 2685, doi: [10.1093/mnras/stz1371](https://doi.org/10.1093/mnras/stz1371)
- Frebel, A. 2018, Annual Review of Nuclear and Particle Science, 68, 237, doi: [10.1146/annurev-nucl-101917-021141](https://doi.org/10.1146/annurev-nucl-101917-021141)
- Frebel, A., & Norris, J. E. 2015, ARA&A, 53, 631, doi: [10.1146/annurev-astro-082214-122423](https://doi.org/10.1146/annurev-astro-082214-122423)
- Frebel, A., Simon, J. D., & Kirby, E. N. 2014, ApJ, 786, 74, doi: [10.1088/0004-637X/786/1/74](https://doi.org/10.1088/0004-637X/786/1/74)
- Fukugita, M., Ichikawa, T., Gunn, J. E., et al. 1996, AJ, 111, 1748, doi: [10.1086/117915](https://doi.org/10.1086/117915)
- Gaia Collaboration, Brown, A. G. A., Vallenari, A., et al. 2021, A&A, 649, A1, doi: [10.1051/0004-6361/202039657](https://doi.org/10.1051/0004-6361/202039657)
- Gaia Collaboration, Vallenari, A., Brown, A. G. A., et al. 2023, A&A, 674, A1, doi: [10.1051/0004-6361/202243940](https://doi.org/10.1051/0004-6361/202243940)
- Gull, M., Frebel, A., Cain, M. G., et al. 2018, ApJ, 862, 174, doi: [10.3847/1538-4357/aacbc3](https://doi.org/10.3847/1538-4357/aacbc3)
- Gunn, J. E., Carr, M., Rockosi, C., et al. 1998, AJ, 116, 3040, doi: [10.1086/300645](https://doi.org/10.1086/300645)
- Gustafsson, B., Edvardsson, B., Eriksson, K., et al. 2008, A&A, 486, 951, doi: [10.1051/0004-6361:200809724](https://doi.org/10.1051/0004-6361:200809724)
- Hansen, T. T., Andersen, J., Nordström, B., et al. 2016a, A&A, 588, A3, doi: [10.1051/0004-6361/201527409](https://doi.org/10.1051/0004-6361/201527409)
- . 2016b, A&A, 586, A160, doi: [10.1051/0004-6361/201527235](https://doi.org/10.1051/0004-6361/201527235)
- Harris, C. R., Millman, K. J., van der Walt, S. J., et al. 2020, Nature, 585, 357, doi: [10.1038/s41586-020-2649-2](https://doi.org/10.1038/s41586-020-2649-2)
- Howes, L. M., Asplund, M., Casey, A. R., et al. 2014, MNRAS, 445, 4241, doi: [10.1093/mnras/stu1991](https://doi.org/10.1093/mnras/stu1991)
- Howes, L. M., Casey, A. R., Asplund, M., et al. 2015, Nature, 527, 484, doi: [10.1038/nature15747](https://doi.org/10.1038/nature15747)
- Howes, L. M., Asplund, M., Keller, S. C., et al. 2016, MNRAS, 460, 884, doi: [10.1093/mnras/stw1004](https://doi.org/10.1093/mnras/stw1004)
- Hunter, J. D. 2007, Computing in Science & Engineering, 9, 90, doi: [10.1109/MCSE.2007.55](https://doi.org/10.1109/MCSE.2007.55)
- Ji, A. P., Li, T. S., Simon, J. D., et al. 2020, ApJ, 889, 27, doi: [10.3847/1538-4357/ab6213](https://doi.org/10.3847/1538-4357/ab6213)
- Ji, A. P., Chandra, V., Mejias-Torres, S., et al. 2025, arXiv e-prints, arXiv:2509.21643, doi: [10.48550/arXiv.2509.21643](https://doi.org/10.48550/arXiv.2509.21643)
- Jorissen, A., Van Eck, S., Van Winckel, H., et al. 2016, A&A, 586, A158, doi: [10.1051/0004-6361/201526992](https://doi.org/10.1051/0004-6361/201526992)

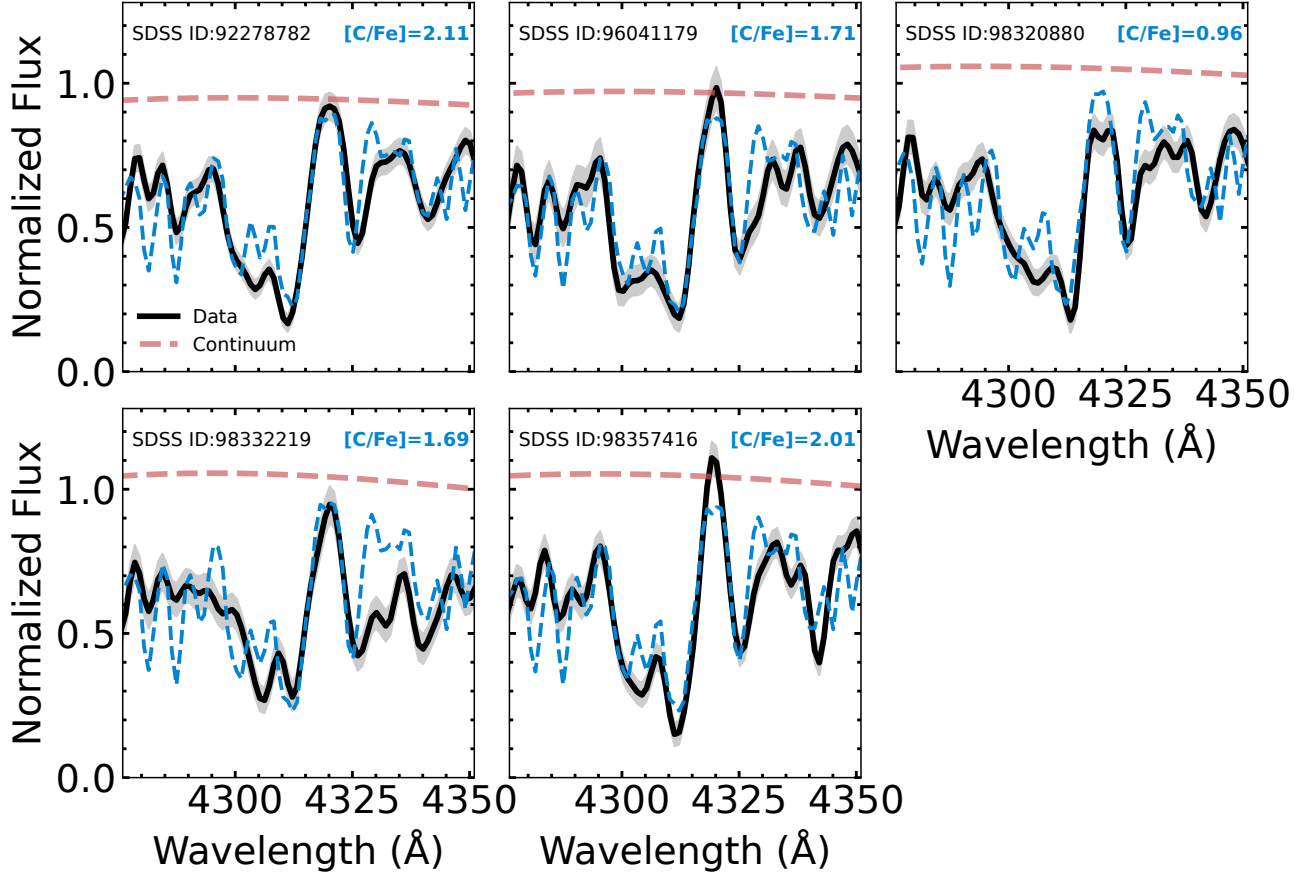


Figure 8. The fits to the CH G-band for the five CEMP stars. The black line with the grey shaded region give the observed normalized flux and the corresponding uncertainty. The blue dashed lines are the best fit synthetic spectra. As the fit is highly sensitive to the continuum normalization, we fit the model continuum to best match the observed spectra. The red dashed line gives the continuum normalization for the best-fit carbon abundance model.

- Kim, S., Staveley-Smith, L., Dopita, M. A., et al. 1998, ApJ, 503, 674, doi: [10.1086/306030](https://doi.org/10.1086/306030)
- Kollmeier, J. A., Rix, H.-W., Aerts, C., et al. 2026, AJ, 171, 52, doi: [10.3847/1538-3881/ae0576](https://doi.org/10.3847/1538-3881/ae0576)
- Kurucz, R. L. 1970, SAO Special Report, 309
- . 1993, SYNTHE spectrum synthesis programs and line data
- Kurucz, R. L., & Avrett, E. H. 1981, SAO Special Report, 391
- Lai, D. K., Lee, Y. S., Bolte, M., et al. 2011, ApJ, 738, 51, doi: [10.1088/0004-637X/738/1/51](https://doi.org/10.1088/0004-637X/738/1/51)
- Lee, Y. S., Beers, T. C., Masseron, T., et al. 2013, AJ, 146, 132, doi: [10.1088/0004-6256/146/5/132](https://doi.org/10.1088/0004-6256/146/5/132)
- Limberg, G., Placco, V. M., Ji, A. P., et al. 2025, ApJL, 989, L18, doi: [10.3847/2041-8213/adf196](https://doi.org/10.3847/2041-8213/adf196)
- Limberg, G., Santucci, R. M., Rossi, S., et al. 2021, ApJ, 913, 11, doi: [10.3847/1538-4357/abeefe](https://doi.org/10.3847/1538-4357/abeefe)

- Lucatello, S., Beers, T. C., Christlieb, N., et al. 2006, ApJL, 652, L37, doi: [10.1086/509780](https://doi.org/10.1086/509780)
- Lucatello, S., Tsangarides, S., Beers, T. C., et al. 2005, ApJ, 625, 825, doi: [10.1086/428104](https://doi.org/10.1086/428104)
- Lucchesi, R., Jablonka, P., Skúladóttir, Á., et al. 2024, A&A, 686, A266, doi: [10.1051/0004-6361/202348093](https://doi.org/10.1051/0004-6361/202348093)
- Lucey, M., Hawkins, K., Ness, M., et al. 2022, MNRAS, 509, 122, doi: [10.1093/mnras/stab2878](https://doi.org/10.1093/mnras/stab2878)
- Lucey, M., Al Kharusi, N., Hawkins, K., et al. 2023, MNRAS, 523, 4049, doi: [10.1093/mnras/stad1675](https://doi.org/10.1093/mnras/stad1675)
- Lugaro, M., Karakas, A. I., Stancliffe, R. J., & Rijs, C. 2012, ApJ, 747, 2, doi: [10.1088/0004-637X/747/1/2](https://doi.org/10.1088/0004-637X/747/1/2)
- Mainzer, A., Bauer, J., Cutri, R. M., et al. 2014, ApJ, 792, 30, doi: [10.1088/0004-637X/792/1/30](https://doi.org/10.1088/0004-637X/792/1/30)
- McClure, R. D., & Woodsworth, A. W. 1990, ApJ, 352, 709, doi: [10.1086/168573](https://doi.org/10.1086/168573)
- Meynet, G., Ekström, S., & Maeder, A. 2006, A&A, 447, 623, doi: [10.1051/0004-6361:20053070](https://doi.org/10.1051/0004-6361:20053070)

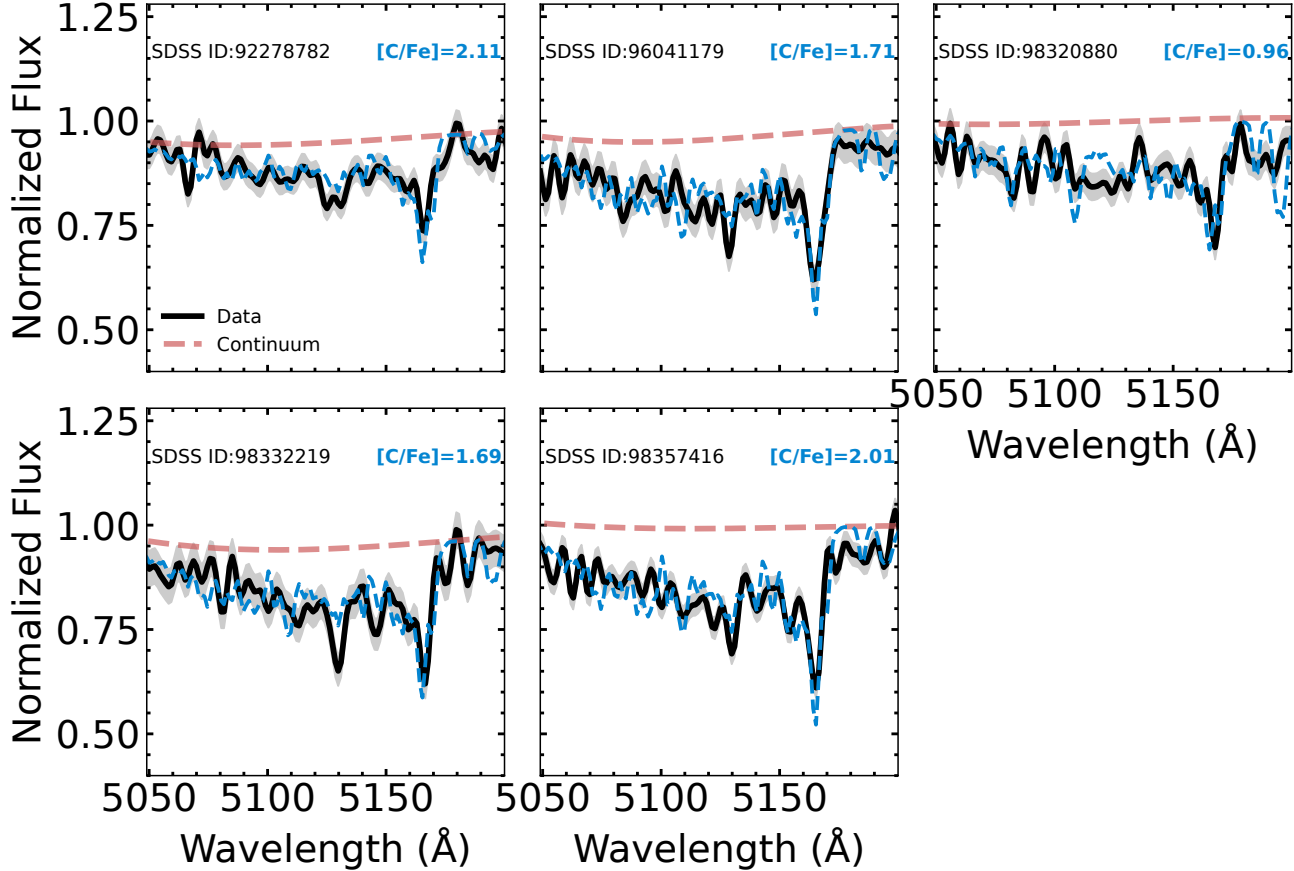


Figure 9. Same as Figure 8, but for the strongest C₂ Swan band.

Nidever, D. L., Majewski, S. R., & Butler Burton, W. 2008, ApJ, 679, 432, doi: [10.1086/587042](https://doi.org/10.1086/587042)

Nidever, D. L., Hasselquist, S., Hayes, C. R., et al. 2020, ApJ, 895, 88, doi: [10.3847/1538-4357/ab7305](https://doi.org/10.3847/1538-4357/ab7305)

Nomoto, K., Kobayashi, C., & Tominaga, N. 2013, ARA&A, 51, 457, doi: [10.1146/annurev-astro-082812-140956](https://doi.org/10.1146/annurev-astro-082812-140956)

Norris, J. E., Wyse, R. F. G., Gilmore, G., et al. 2010, ApJ, 723, 1632, doi: [10.1088/0004-637X/723/2/1632](https://doi.org/10.1088/0004-637X/723/2/1632)

Pérez, F., & Granger, B. E. 2007, Computing in Science and Engineering, 9, 21, doi: [10.1109/MCSE.2007.53](https://doi.org/10.1109/MCSE.2007.53)

Placco, V. M., Frebel, A., Beers, T. C., et al. 2013, ApJ, 770, 104, doi: [10.1088/0004-637X/770/2/104](https://doi.org/10.1088/0004-637X/770/2/104)

Placco, V. M., Frebel, A., Beers, T. C., & Stancliffe, R. J. 2014, ApJ, 797, 21, doi: [10.1088/0004-637X/797/1/21](https://doi.org/10.1088/0004-637X/797/1/21)

Placco, V. M., Beers, T. C., Santucci, R. M., et al. 2018, AJ, 155, 256, doi: [10.3847/1538-3881/aac20c](https://doi.org/10.3847/1538-3881/aac20c)

Placco, V. M., Limberg, G., Chiti, A., et al. 2025, ApJ, 991, 101, doi: [10.3847/1538-4357/adf846](https://doi.org/10.3847/1538-4357/adf846)

Plez, B. 2012, Turbospectrum: Code for spectral synthesis, Astrophysics Source Code Library.

<http://ascl.net/1205.004>

Preston, G. W., & Sneden, C. 2001, AJ, 122, 1545, doi: [10.1086/322082](https://doi.org/10.1086/322082)

Price-Whelan, A., Garrison, L., Souchereau, H., et al. 2025, adrnl/gala: v1.10.1, v1.10.1, Zenodo, doi: [10.5281/zenodo.16923466](https://doi.org/10.5281/zenodo.16923466)

Price-Whelan, A. M. 2017, The Journal of Open Source Software, 2, doi: [10.21105/joss.00388](https://doi.org/10.21105/joss.00388)

Reggiani, H., Schlaufman, K. C., Casey, A. R., Simon, J. D., & Ji, A. P. 2021, AJ, 162, 229, doi: [10.3847/1538-3881/ac1f9a](https://doi.org/10.3847/1538-3881/ac1f9a)

Rossi, S., Beers, T. C., & Sneden, C. 1999, in Astronomical Society of the Pacific Conference Series, Vol. 165, The Third Stromlo Symposium: The Galactic Halo, ed. B. K. Gibson, R. S. Axelrod, & M. E. Putman, 264

Ryabchikova, T., Piskunov, N., Kurucz, R. L., et al. 2015, PhyS, 90, 054005, doi: [10.1088/0031-8949/90/5/054005](https://doi.org/10.1088/0031-8949/90/5/054005)

Salvadori, S., Skúladóttir, Á., & Tolstoy, E. 2015, MNRAS, 454, 1320, doi: [10.1093/mnras/stv1969](https://doi.org/10.1093/mnras/stv1969)

- Sestito, F., Ardern-Arentsen, A., Vitali, S., et al. 2024, *A&A*, 690, A333, doi: [10.1051/0004-6361/202451258](https://doi.org/10.1051/0004-6361/202451258)
- Shipp, N., Erkal, D., Drlica-Wagner, A., et al. 2021, *ApJ*, 923, 149, doi: [10.3847/1538-4357/ac2e93](https://doi.org/10.3847/1538-4357/ac2e93)
- Skrutskie, M. F., Cutri, R. M., Stiening, R., et al. 2006, *AJ*, 131, 1163, doi: [10.1086/498708](https://doi.org/10.1086/498708)
- Skúladóttir, Á., Tolstoy, E., Salvadori, S., et al. 2015, *A&A*, 574, A129, doi: [10.1051/0004-6361/201424782](https://doi.org/10.1051/0004-6361/201424782)
- Smee, S. A., Gunn, J. E., Uomoto, A., et al. 2013, *AJ*, 146, 32, doi: [10.1088/0004-6256/146/2/32](https://doi.org/10.1088/0004-6256/146/2/32)
- Starkenburg, E., Shetrone, M. D., McConnachie, A. W., & Venn, K. A. 2014, *MNRAS*, 441, 1217, doi: [10.1093/mnras/stu623](https://doi.org/10.1093/mnras/stu623)
- Tominaga, N., Iwamoto, N., & Nomoto, K. 2014, *ApJ*, 785, 98, doi: [10.1088/0004-637X/785/2/98](https://doi.org/10.1088/0004-637X/785/2/98)
- Umeda, H., & Nomoto, K. 2003, *Nature*, 422, 871, doi: [10.1038/nature01571](https://doi.org/10.1038/nature01571)
- van der Marel, R. P., Alves, D. R., Hardy, E., & Suntzeff, N. B. 2002, *AJ*, 124, 2639, doi: [10.1086/343775](https://doi.org/10.1086/343775)
- Virtanen, P., Gommers, R., Oliphant, T. E., et al. 2020, *Nature Methods*, 17, 261, doi: [10.1038/s41592-019-0686-2](https://doi.org/10.1038/s41592-019-0686-2)
- Watkins, L. L., van der Marel, R. P., & Bennet, P. 2024, *ApJ*, 963, 84, doi: [10.3847/1538-4357/ad1f58](https://doi.org/10.3847/1538-4357/ad1f58)
- Yoon, J., Beers, T. C., Placco, V. M., et al. 2016, *ApJ*, 833, 20, doi: [10.3847/0004-637X/833/1/20](https://doi.org/10.3847/0004-637X/833/1/20)
- Yoon, J., Beers, T. C., Dietz, S., et al. 2018, *ApJ*, 861, 146, doi: [10.3847/1538-4357/aaccea](https://doi.org/10.3847/1538-4357/aaccea)
- Zepeda, J., Beers, T. C., Placco, V. M., et al. 2023, *ApJ*, 947, 23, doi: [10.3847/1538-4357/acbbcc](https://doi.org/10.3847/1538-4357/acbbcc)